Journal of Materials Chemistry A

Hybrid material based on coordination complex modified polyoxometalate nanorod (CC/POMNR) and PPy: A new visible light active and high efficient photocatalyst

Journal:	*Journal of Materials Chemistry A*
Manuscript ID:	TA-ART-09-2014-005071.R1
Article Type:	Paper
Date Submitted by the Author:	19-Oct-2014
Complete List of Authors:	xu, xinxin; Inorganic Institution, Chemistry Department Gao, Xin; Inorganic Institution, Chemistry Department Lu, Tingting; Inorganic Institution, Chemistry Department Liu, Xiaoxia; Inorganic Institution, Chemistry Department Wang, Xiuli; Bohai University, Faculty of Chemistry and Chemical Engineering

Hybrid material based on coordination complex modified polyoxometalate nanorod (CC/POMNR) and PPy: A new visible light active and high efficient photocatalyst

Xinxin Xu[a], Xin Gao[a], Tingting Lu[a], Xiaoxia Liu*[a] and Xiuli Wang*[b]

[a]*Department of Chemistry, College of Science, Northeast University, Shenyang, Liaoning, 110819, People's Republic of China*

[b]*Department of Chemistry, Bohai University, Jinzhou, Liaoning, 121013, People's Republic of China*

*Author to whom correspondence should be addressed.

Tel: +86-024-83689510, E-mail: xxliu@mail.neu.edu.cn (Professor X. X. Xu)

Tel: +86-0416-3400158, E-mail:wangxiuli@bhu.edu.cn (Professor X. L. Wang)

Abstract

To improve the photocatalytic activity of a coordination complex modified polyoxometalate (**CC/POM**), a new kind of hybrid material (abbreviated as **PPy/CC/POMNR**) was fabricated through the combination of its nanorod (**CC/POMNR**) and polypyrrole (PPy) with a facile in-situ chemical oxidation polymerization process under the initiation of ammonium persulfate (APS). Under irradiation of visible light, **PPy/CC/POMNR** exhibited more excellent photocatalytic activity than **CC/POMNR**, PPy and their mechanically blended products on degradation of Rhodamine B (RhB). Optical and electrochemical tests illustrated the enhancement of photocatalytic performance can be ascribed to high separation efficiency of photogenerated electron and hole on the interface of **CC/POMNBs** and PPy, which resulted from the synergy effect between them. Furthermore, the influence of concentration ration between pyrrole (Py) and APS on morphology, conductivity and photocatalytic property of the **PPy/CC/POMNR** was discussed and an optical condition to fabricate hybrid material with high efficiency had been obtained. These results suggest the hybrid of **CC/POMNR** and PPy would be a feasible strategy to enhance photocatalytic activity of **CC/POMNR**.

Introduction

Recently, serious environmental problem caused by organic dyes accelerates the development of efficient methods for their treatment.[1] In this aspect, photocatalytic degradation has been proved to be a feasible method to decompose these pollutants into less dangerous matter.[2] Because of cleanness and low cost during organic dyes treatment process, **CC/POM**, especially nanoscale coordination complex modified polyoxometalate (**NCC/POM**) has attracted researchers' great interests.[3] Compared with other photocatalysts, the stability of **NCC/POM** is much higher, which makes them more convenient in recovering and recycling.[4] Furthermore, because of its large surface area, **NCC/POM** can contact with organic dyes adequately and urge them decompose more completely.[5] But the drawbacks such as inactive in visible light region (for the wide band gap of **NCC/POM**) as well as low photocatalytic efficiency (caused by quick recombination rate of photogenerated electron and hole during photocatalysis process) still impede further application of **NCC/POM** in waste water treatment.[6, 7] Now, the extension of photoresponse region from ultraviolet to visible light region and the enhancement of photocatalytic efficiency become significant problems in the exploration of **NCC/POM** photocatalyst.

To resolve these problems, the hybrid of **NCC/POM** with a visible light active material, which possesses excellent photogenerated electron-hole pair separation property, may be a feasible strategy. In this aspect, PPy is an ideal choice. At first, its photoresponse region is very broad, which ranges from ultraviolet to visible light region.[8] Secondly, as an excellent photogenerated hole transporting material, PPy can separate electron-hole pair effectively and impede recombination of electron and hole again, which can enhance the photocatalytic efficiency.[9] More importantly, the polymerization condition of PPy is mild and this will prevent the decomposition of

NCC/POM during fabrication process of the hybrid material.[10] By now, PPy has been applied enhance the photocatalytic property of some typical photocatalysts, such as TiO_2 and ZnO, which has received very favorable results.[11-15] Encouraged by these, we want to improve the photocatalytic property of **NCC/POM** through its hybrid with PPy.

Our imagination was confirmed to be reasonable by a visible light active photocatalyst **PPy/ZnP$_2$Mo$_5$NR**, which was synthesized by the hybrid of PPy and nanorods of a new **CC/POM**, $\{[Zn(PyBim)_2(H_2O)(P_2Mo_5O_{23})]\cdot(H_2PyBim)_2\cdot(H_2O)_5\}_n$ (**ZnP$_2$Mo$_5$**, PyBim = 2-(3-pyridyl)benzimidazole). Photocatalytic degradation of RhB was investigated and results indicated the hybrid of **ZnP$_2$Mo$_5$NR** and PPy enhanced its photocatalytic property effectively. During polymerization of PPy, the concentration ration between Py and APS (abbreviated as [Py]/[APS]) has great effects on its chemical and physical properties, which may further influence photocatalytic of the resulted **PPy/ZnP$_2$Mo$_5$NR** hybrid material.[16] To make this point clear, in-situ chemical oxidative polymerization of Py was conducted under different conditions and an optical [Py]/[APS] value to achieve **PPy/ZnP$_2$Mo$_5$NR** with excellent photocatalytic activity was obtained.

Experimental section

Materials and synthesis

All purchased chemicals were of reagent grade and used without further purification. Elemental analyses (C, H and N) were performed on a Perkin–Elmer 2400 CHN Elemental Analyzer. P, Mo and Zn were determined with a Leeman inductively coupled plasma (ICP) spectrometer. The morphology was observed on an ultra plus field emission scanning electron microscope (ZEISS, Germany). PXRD patterns were recorded on D8 X-ray diffractometer, employing monochromatized Cu

Kα incident radiation. FTIR spectra were recorded in the range 4000-400 cm^{-1} on an Alpha Centaur FTIR spectrophotometer using KBr pellets. Diffuse reflectance spectra (DRS) were recorded on a Shimadzu-2501PC spectrometer using $BaSO_4$ as a standard. The conductivity measurement was performed by conventional four-probe technique. Electrochemical experiments were conducted on CHI 660E electrochemical workstation. The UV-visible adsorption spectrum was recorded using a Hitachi U-3010 UV-visible spectrometer.

Synthesis of $\{[Zn(PyBim)_2(H_2O)(P_2Mo_5O_{23})]\cdot(H_2PyBim)_2\cdot(H_2O)_5\}_n$ (ZnP_2Mo_5)

ZnP_2Mo_5 was prepared from the mixture of $Zn(OAc)_2\cdot 2H_2O$ (0.022 g, 0.1 mmol), PyBim (0.019 g, 0.1 mmol), $Na_2MoO_4\cdot 2H_2O$ (0.048 g, 0.2 mmol), H_3PO_4 (0.1 ml) and 5 mL H_2O. The mixture was stirred for 10 minutes and then transferred to a 15 mL Teflon-lined stainless steel bomb and kept at 180˚C under autogenously pressure for 4 days. The reaction system was cooled to room temperature during 24 hours. A large amount of yellow crystals of **ZnP_2Mo_5** were obtained. Yield: 81% (based on Zn). Anal. Calcd for $C_{48}H_{52}N_{12}O_{29}ZnP_2Mo_5$: C, 30.86%; H, 2.81%; N, 8.99%; P, 3.32%; Mo, 25.68%; Zn, 3.50%. Found: C, 30.73%; H, 2.92%; N, 9.03%; P, 3.42%; Mo, 25.54%; Zn, 3.38%.

Synthesis of ZnP_2Mo_5NR

The crystals of **ZnP_2Mo_5** were grinded for 4 hours with an agate mortar and pestle. The resulted powder was dissolved in methanol and placed in a Teflon autoclave, which was heated in a microwave oven at 400 W for 2 hours. The resulted **ZnP_2Mo_5NR** were separated by centrifugation, rinsed with water and then dried in a vacuum at 70 ˚C for 24 hours.

Synthesis of PPy/ZnP_2Mo_5NR hybrid material

Py (0.034 g, 5 x 10^{-4} mol) was dissolved in 20 mL H_2O. **ZnP_2Mo_5NR** (4.671 g, 2.5

x 10^{-3} mol) was also placed in above solution and dispersed with supersonic for 25 minutes. 10 ml APS solution was slowly added to above mixture as oxidant. The product was stirred for 20 minutes and left undisturbed for 12 hours. The resulting **PPy/ZnP_2Mo_5NR** hybrid material was separated, rinsed with water, alcohol and finally dried at 60˚C for 24 hours in an oven. In the experiment, hybrid material was prepared with the ratio of [Py]:[APS] equal to 4:1, 2:1, 1:1 and 1:2. The products were labeled as **PPy(A)/ZnP_2Mo_5NR**, **PPy(B)/ZnP_2Mo_5NR**, **PPy(C)/ZnP_2Mo_5NR** and **PPy(D)/ZnP_2Mo_5NR** respectively.

Synthesis of PPy and **PPy/ZnP_2Mo_5NR(M)**

PPy(A) to PPy(D) were obtained through a similar process with **PPy/ZnP_2Mo_5NR** hybrid material, except **ZnP_2Mo_5NR** was not added. **PPy(A)/ZnP_2Mo_5NR(M)** to **PPy(D)/ ZnP_2Mo_5NR(M)** were synthesized by the mixing of PPy and **ZnP_2Mo_5NR** directly.

Photocatalytic activity study

The photocatalytic activities of samples were evaluated by the degradation of RhB in the aqueous solution. 80 ml RhB aqueous solution with concentration of 10^{-5} M was mixed with 20 mg catalysts, which was exposed to illumination. Before turning on the lamp, the suspension containing RhB and photocatalyst were magnetically stirred in a dark condition for 40 min till an adsorption-desorption equilibrium was established. Samples were then taken out regularly from the reactor and centrifuged immediately for separation of any suspended solid. The transparent solution was analyzed by a UV-vis spectrometer. A 300 W medium pressure mercury lamp served as an ultraviolet light source and a 300 W Xe lamp with a cutoff filter ($\lambda \geq 420$ nm) served as a visible light source.

Electrochemical measurements

Photoelectrochemical tests were carried out with a conventional three-electrode system in quartz cell filled with 0.1 M Na_2SO_4 electrolyte (100 mL). The **ZnP_2Mo_5NR/ITO** or **PPy/ZnP_2Mo_5NR/ITO** electrodes served as the working electrode. The counter and reference electrodes were a Pt plate and a saturated calomel electrode (SCE), respectively. A 300 W Xe lamp with a cutoff filter ($\lambda \geq 420$ nm) were used as the excitation light source for visible irradiation. Electrochemical impedance spectra (EIS) were recorded in potentiostatic mode. The amplitude of sinusoidal wave was 10 mV, and the frequency range of the sinusoidal wave was from 100 kHz to 0.05 Hz.

X-ray crystallography

Suitable single crystal of **ZnP_2Mo_5** was carefully selected under an optical microscope and glued on glass fiber. Structural measurement was performed on a Bruker AXS SMART APEX II CCD diffractometer at 293 K. The structure was solved by the direct method and refined by the full-matrix least-squares method on F^2 using the SHELXTL 97 crystallographic software package.[17] Anisotropic thermal parameters were used to refine all non-hydrogen atoms. Carbon-bound hydrogen atoms were placed in geometrically calculated positions; Oxygen-bound hydrogen atoms were located in the difference Fourier maps, kept in that position and refined with isotropic temperature factors. The X-ray structural analysis is listed in Table S1. Selected bond lengths are listed in Table S2. Selected bond angles are listed in Table S3. Further details of the crystal structure have been deposited to the Cambridge Crystallographic Data Centre as supplementary publication, which can be obtain free of charge (CCDC 1017803). The Cambridge Crystallographic Data Centre via www.ccdc.cam.ac.uk/data_request/cif.

Structure and morphology study

Single crystal X-ray analysis reveals the fundamental unit of **ZnP_2Mo_5** is made up by one standberg type polyanion $[P_2Mo_5O_{23}]^{6-}$ (abbreviated as P_2Mo_5), one Zn(II) cation, two PyBim ligands and one coordinated water molecule. The P_2Mo_5 cluster is similar with standberg polyanion in other **CC/POMs**, which can be described as a ring of five distorted MoO_6 octahedron with two PO_4 tetrahedron capped on each side.[18] Each phosphate subunit shares three oxo-groups with the molybdate ring, in which one of these oxo-groups adopts the μ_2-bridging mode, while the other two adopt the μ_3-bridging mode. In this P_2Mo_5 cluster, Mo-O_b bond distances range from 2.210(5) to 2.425(5) Å, Mo-O_c bond distances are in the range of 1.863(5) to 1.961(5) Å and Mo-O_d bond distance range from 1.698(5) to 1.731(6) Å. The P-O bond distances vary from 1.522(5) to 1.568(5) Å and O-P-O band angles are in the range of 106.4(3) to 112.6(3)˚. The adjacent P_2Mo_5 clusters are connected by $[Zn(PyBim)_2(H_2O)]$ unit with Zn1-O1 = 1.980(5) Å and Zn1-O22 = 1.982(5) Å, which results 1D chain like structure of **ZnP_2Mo_5** (Fig. 1a). The morphology of **ZnP_2Mo_5NR** was studied with SEM. The surface of **ZnP_2Mo_5NR** is very smooth, its length and width of both range from 60 to 80 nm, while its height vary from 0.8 to 1.5 μm (Fig. 1b).

The morphologies of **PPy/ZnP_2Mo_5NR** hybrid materials were also studied with SEM. It can be observed clearly, **PPy** particles are located evenly around **ZnP_2Mo_5NR**. In hybrid materials, the dimension and element contents of **ZnP_2Mo_5NR** are similar with pure **ZnP_2Mo_5NR**, which illustrates its morphology and structure are not altered during the polymerization process of Py. As [Py]/[APS] = 4, **ZnP_2Mo_5NR** are surrounded by PPy nanoparticles with diameter about 30 to 40 nm (Fig. 2a). If [Py]/[APS] value decreases, besides these small PPy particles, some large PPy nanoparticles with diameter 200 to 300 nm appear around **ZnP_2Mo_5NR** (Fig. 2b

and 2c). When [Py]/[APS] = 0.5, small PPy particles disappear completely, only PPy particles with large size are left (Fig. 2d). The alteration of morphology can be ascribed to the influence of [Py]/[APS] value. When [Py]/[APS] = 4, [APS] is insufficient, this leads to a slow polymerization process of Py, which results PPy with small size. As [APS] increased, polymerization process is speeded up; this leads to the secondary polymerization of Py on early resulted PPy, which usually results PPy particles with larger size.

PXRD was employed to study the structures of **ZnP_2Mo_5NR** and **PPy/ZnP_2Mo_5NR** (Fig. 3a and 3b). **ZnP_2Mo_5NR** and **PPy/ZnP_2Mo_5NR** take on similar diffraction patterns with **ZnP_2Mo_5**, which illustrates in **ZnP_2Mo_5NR** and **PPy/ZnP_2Mo_5NR** the structures of **ZnP_2Mo_5** are still retained. Furthermore, the peaks belong to PPy are not observed, which illustrates the content of PPy may be too small to determine its existence.[19] In these hybrid materials, to study the interactions between **ZnP_2Mo_5NR** and PPy, FTIR spectra were employed. In **ZnP_2Mo_5NR**, the characteristic bands at 818, 921 and 1052 cm^{-1} can be attributed to the stretching of Mo-O_b-Mo, Mo-O_d and P-O_a respectively.[20] As for **PPy/ZnP_2Mo_5NR**, these peaks move to higher wavenumber region (Fig. 3c and 3d). On the contrary, the N-H stretching of PPy move to lower wavenumber region compared with pure PPy. All these movements reveal effective interactions between **ZnP_2Mo_5NR** and PPy, which can be ascribed to the existence of hydrogen bonds and π-π interactions.[21]

Optical property

The UV-vis diffuse reflectance spectra (DRS) of **ZnP_2Mo_5NR** and **PPy/ZnP_2Mo_5NR** hybrid materials were studied. Compared with visible light inactive **ZnP_2Mo_5NR**, **PPy/ZnP_2Mo_5NR** hybrid materials show strong photoresponse in ultraviolet and visible light region, which suggests PPy is a suitable option to extend

the photoresponse region of **ZnP_2Mo_5NR** (Fig. 4a). To study influences of the ratio of [Py]:[APS] on photoresponse region in detail, band gaps (E_g) of **ZnP_2Mo_5NR** and **PPy/ZnP_2Mo_5NR** hybrid materials were obtained from Tauc equation (Fig. 4b). We find with decreasing of the ratio of [Py]:[APS], E_g of the hybrid material become narrower. If the ratio of [Py]:[APS] decreases continuously, the opposite situation occurs. In these hybrid materials, **PPy(C)/ZnP_2Mo_5NR** possesses the narrowest band gap, which illustrates the ratio of [Py]:[APS] = 1 is an optical condition to fabricate hybrid material with more extensive photoresponse region.

Electrochemical analysis

The interface charge separation efficiency can be investigated by photocurrent spectra and electrochemical impedance spectroscopy (EIS). Photocurrent responses were conducted under irradiation of ultraviolet and visible light. We can observe clearly **ZnP_2Mo_5NR/ITO** electrode only exhibit photocurrent response under ultraviolet light (Fig. 5a). On the contrary, **PPy/ZnP_2Mo_5NR/ITO** electrodes show strong photocurrent response under both ultraviolet and visible light irradiation. Their photocurrents both rapidly decrease to zero when light is switched off (Fig. 5b). This indicates the hybrid of PPy and **ZnP_2Mo_5NR** can enhance its photocurrent effectively. Furthermore, with increasing of the ratio of [Py]:[APS], photocurrent of **PPy/ZnP_2Mo_5NR/ITO** electrodes increase at first and then decrease. **PPy(C)/ZnP_2Mo_5NR/ITO** electrode exhibited the largest photocurrent.

To study the charge separation and transfer process in detail, EIS was employed (Fig. 5c and 5d). In EIS, the radius of the *arc* on Nynquist plot reflects the reaction rate occurred on the surface of the electrode.[22] The *arc* radius of all the **PPy/ZnP_2Mo_5NR/ITO** electrodes are smaller than **ZnP_2Mo_5NR/ITO** electrode, which illustrates a more effective separation of photogenerated electron-hole pair as

well as a faster interfacial charge transfer have occurred after the introduction of PPy. In the hybrid material electrodes, **PPy(C)/ZnP_2Mo_5NR/ITO** electrode exhibits smallest *arc* radius, which implies it possesses the highest photogenerated charge separation efficiency.

In summary, these electrochemical tests are matched well with the optical property studies. All these results indicate the hybrid of PPy and **ZnP_2Mo_5NR** decreases the recombination of photogenerated electron-hole pair. Furthermore, compared with other values, the ratio of [Py]:[APS] =1 is a more appropriate condition to fabricate hybrid material with excellent electron-hole pair separation efficiency.

Photocatalytic property study

The photocatalytic activities of **ZnP_2Mo_5NR** and **PPy/ZnP_2Mo_5NR** hybrid materials were evaluated by the degradation of RhB in aqueous solution. Like other **CC/POM** photocatalysts, as an ultraviolet light active photocatalyst, **ZnP_2Mo_5NR** exhibits no effect on RhB in visible light region (Fig. 6a). On the contrary, its hybrid materials show more excellent photocatalytic activities in visible light region (Fig. 6b). We deduce the enhancement of photocatalytic activity originates from the synergy between PPy and **ZnP_2Mo_5NR**. To illustrate this point clearly, PPy and **PPy/ZnP_2Mo_5NR(M)** (mechanically blended product of PPy and **ZnP_2Mo_5NR**) were used as reference to evaluate the photocatalytic efficiency (Fig. 6c and 6d). It is notable their photocatalytic efficiency are much less than **PPy/ZnP_2Mo_5NR** hybrid materials. This implies the synergy between PPy and **ZnP_2Mo_5NR** dose play a crucial role in the improvement of photocatalytic activity.

Furthermore, we also find with the increasing of the ratio of [Py]:[APS], photocatalytic activities of **PPy/ZnP_2Mo_5NR** hybrid materials did not raise monotonously. This can be also ascribed to the difference in conductivity of PPy (Fig.

7a). As the ratio of [Py]:[APS] > 1, [APS] is insufficient, which can not oxide Py completely. This will produce PPy with low molecular weight and poor conductivity, which can not separate photogenerated electron-hole pair effectively. With the increasing of oxidant, PPy with high molecular weight and conductivity is obtained, which can separate photogenerated electron-hole pair more effectively. As the ratio of [Py]:[APS] = 1, we obtain **PPy(C)/ ZnP_2Mo_5NR**, which exhibits the best performance during photocatalytic decomposition of RhB. If [APS] increases continuous, excess APS can destroy π-conjugated structure of PPy reduce its conductivity and electron-hole pair separation ability. So, in these hybrid materials, **PPy(C)/ZnP_2Mo_5NR** exhibits highest photocatalytic efficiency. This is in accordance with the optical and electrochemical studies.

In photocatalytic degradation reaction, the activity and stability of recycled catalyst are very important factors to determine the performance of a photocatalyst. Herein, photocatalytic property of **PPy(C)/ZnP_2Mo_5NR** are re-examined for five times and the recycled photocatalysts still show excellent photocatalytic properties (Fig. 7b). Furthermore, the recycled sample also exhibits similar PXRD and FTIR patterns with original hybrid material, which indicates the structure of **PPy(C)/ZnP_2Mo_5NR** is not destroyed during the photocatalysis process (Fig.7c and 7d).

Mechanism study

In order to study the intrinsic electronic property of **PPy**/**ZnP_2Mo_5NR** hybrid material, Mott-Schotty measurement had been applied in darkness using impedance technique. We studied the capacitance measurement in the Mott-Schotty-type plot for **ZnP_2Mo_5NR** (Fig. 8a). The positive slope of the obtained C^{-2}/E plot illustrates **ZnP_2Mo_5NR** belongs to typical n-type semiconductors.[23] The conductive band potential can also be obtained from this method, which is -0.4 V (vs SCE). Combined

with band gap (E_g) estimated from DRS, the valence band (VB) of **ZnP_2Mo_5NR** is calculated to be 2.72V (vs SCE) according to the formula: $E_{VB} = E_{CB} + E_g$.

Based on these results and experimental findings, we speculate the mechanism of **PPy**/**ZnP_2Mo_5NR** hybrid material as follows. For **PPy**/**ZnP_2Mo_5NR**, its valence band (VB) and conduction band (CB) match well with the lowest unoccupied molecular orbital (LUMO) and highest occupied molecular orbital (HOMO) of PPy (Fig 8b). So, under visible light irradiation, only PPy is excited and produces electron on its LUMO orbital, and then the electron transfers into the CB of **ZnP_2Mo_5NR**, at the same time, the hole is born on VB of **ZnP_2Mo_5NR** and inject to HOMO of PPy. This process leads to the charge separation and stabilization, which hinders the recombination of electrons and holes. Based on aforementioned points, in **PPy**/**ZnP_2Mo_5NR** hybrid material, the role of PPy can be described as efficient electron donor and good hole transporter.

Conclusions

PPy/CC/POMNR hybrid material was fabricated successfully through the in-situ chemical polymerization of Py with the existence of **CC/POMNR**. As expected, compared with **CC/POMNR**, PPy and their mechanically blended product, the hybrid material exhibits much higher photocatalytic efficiency under irradiation of visible light. We also discussed influence of the ratio of [Py]:[APS] on morphology, conductivity and photocatalytic activity of the hybrid material and an optical value had been obtained. The preparation of **PPy/CC/POMNR** enables us to establish a rational strategy to improve photocatalytic performance of **POM** based photocatalyst. Furthermore, **PPy/CC/POMNR** is a new kind of efficient photocatalyst for decontaminating colored wastewater produced in textile industries production.

Acknowledgements

This work was supported by National Natural Science Foundation of China (21303010, 21273029 and 21471021); Research Foundation for the Doctoral Program of Higher Education of China (20120042110024); Fundamental Research Funds for the Central Universities (N120405005).

Electronic supplementary information (ESI) available: Crystal data and structure refinement results, selected bond lengths and angles of **ZnP_2Mo_5**. Absorption spectra of RhB degraded with **ZnP_2Mo_5NR** under irradiation of ultraviolet and visible light; Absorption spectra of RhB degraded with **PPy/ZnP_2Mo_5NR**, PPy and **PPy/ZnP_2Mo_5NR(M)** under irradiation of visible light.

Reference

1 (a) R. Asahi, T. Morikawa, T. Ohwaki, K. Aoki and Y. Taga, *Science* 2001, **293**, 269; (b) W. Zhao, W. H. Ma, C. C. Chen, J. C. Zhao and Z. G. Shuai, *J. Am. Chem. Soc*., 2004, **126**, 4782; (c) Y. Cong, J. L. Zhang, F. Chen and M. Anpo, *J. Phys. Chem*., *C* 2007, **111**, 6976.

2 (a) S. Kohtani, M. Koshiko, A. Kudo, K. Tokumura, Y. Ishigaki, A. Toriba, K. Hayakawa and R. Nakagaki, *Appl. Catal., B* 2003, **46**, 573; (b) S. Kohtani, M. Tomohiro, K. Tokumura and R. Nakagaki, *Appl. Catal., B* 2005, **58**, 265; (c) X. H. Lu, S. L. Xie, H. Yang, Y. X. Tong, and H. B. Ji, *Chem. Soc. Rev*., DOI: 10.1039/c3cs60392j.

3 (a) J. X. Meng, Y. G. Li, H. Fu, X. L. Wang and E. B. Wang, *CrystEngComm*., 2011, **13**, 649; (b) K. Wang, D. D. Zhang, J. C. Ma, P. T. Ma, J. Y. Niu and J. P. Wang, *CrystEngComm*., 2012, **14**, 3205; (c) W. Q. Kan, J. Yang, Y. Y. Liu and J. F. Ma, *Dalton Trans*., 2012, **41**, 11062.

4 (a) H. X. Yang, T. F. Liu, M. N. Cao, H. F. Li, S. Y. Gao and R. Cao, *Chem. Commun*., 2010, **46**, 2429; (b) Y. H. Guo and C. W. Hu, *J. Mol. Catal. A: Chem*., 2007, **262**, 136.

5 (a) T. B. Liu, E. Diemann, H. L. Li, A. W. M. Dress and A. Müll, *Nature* 2003, **426**, 59; (b) Z. H. Kang, Y. B. Wang, E. B. Wang, S. Y. Lian, L. Gao, W. S. You, C. W. Hu and L. Xu, *Eur. J. Inorg. Chem*., 2003, 370; (c) Z. H. Kang, Y. B. Wang, E. B. Wang, S. Y. Lian, L. Gao, W. S. You, C. W. Hu and L. Xu, *Solid Stathe Commun*., 2004, **129**, 559.

6 (a) J. X. Meng, Y. Lu, Y. G. Li, H. Fu, X. L. Wang and E. B. Wang, *CrystEngComm*., 2011, **13**, 2479; (b) Y. Ding, J. X. Meng, W. L. Chen and E. B. Wang, *CrystEngComm*., 2011, **13**, 2687; (c) X. L. Wang, Y. F. Wang, G. C. Liu,

A. X. Tian, J. W. Zhang and H. Y. Lin, *Dalton Trans*., 2011, **40**, 9299.

7 (a) J. Y. Niu, S. W. Zhang, H. N. Chen, J. W. Zhao, P. T. Ma and J. P. Wang, *Cryst. Growth Des*., 2011, **11**, 3769; (b) B. F. Meng, W. S. You, X. F. Sun, F. Zhang and M. Y. Liu, *Inorg. Chem. Commun*., 2011, **14**, 35; (c) Y. Q. Jiao, C. Qin, C. Y. Sun, K. Z. Shao, P. J. Liu, P. Huang, K. Zhou and Z. M. Su, *Inorg. Chem. Commun*., 2012, **20**, 273.

8 (a) K. Murakoshi, R. Kogure, Y. Wada and S. Yanagida, *Sol. Energy Mater. Sol. Cells* 1998, **55**, 113; (b) R. Cervini, Y. Cheng and G. Simon, *J. Phys. D: Appl. Phys*., 2004, **37**, 13.

9 (a) T. Kitamura, M. Maitani, M. Matsuda, Y. Wada and S. Yanagida, *Chem. Lett*., 2001, **10**, 1054; (b) D. Chowdhury, A. Paul and A. Chattopadhyay, *Langmuir* 2005, **21**, 4123;

10 (a) Q. L. Li, C. R. Zhang and J. Q. Li, *J. Alloys. Compd*., 2011, **509**, 1953; (b) D. Wang, Y. Wang, X. Li, Q. Luo, J. An and H. Yue, *Catal. Commun*., 2008, **9**, 1162.

11 (a) B. Wang, C. Li, J. F. Pang, X. T. Qing, J. P. Zhai and Q. Li, *Appl. Surf. Sci*., 2012, **258**, 9989; (b) S. N. Gu, B. Li, C. J. Zhao, Y. L. Xu, X. Z. Qian and G. R. Chen, *J. Alloys. Compd*., 2011, **509**, 5677; (c) X. C. Li, G. L. Jiang, G. H. He, W. J. Zheng, Y. Tan and W. Xiao, *Chem. Eng. J*., 2014, **236**, 480.

12 (a) T. A. Kandiel, R. Dillert and D. W. Bahnemann, *Photochem. Photobiol*., 2009, **8**, 683; (b) F. Deng, L. J. Min, X. B. Luo, S. L. Wu and S. L. Luo, *Nanoscale* 2013, **5**, 8703; (c) N. M. Dimitrijevic, S. Tepavcevic, Y. Z. Liu, T. Rajh, S. C. Silver and D. M. Tiede, *J. Phys. Chem. C* 2013, **117**, 15540.

13 (a) G. K. R. Senadeera, T. Kitamura, Y. Wada and S. Yanagida, *J. Photochem. Photobiol. A: Chem*., 2006, **184**, 234; (b) G. K. R. Senadeera, T. Kitamura, Y.

Wada and S. Yanagida, *J. Photochem. Photobiol. A: Chem*., 2004, **164**, 61; (c) X. F. Lu, Q. D. Zhao, X. C. Liu, D. J. Wang, W. J. Zhang, C. Wang and Y. Wei, *Macromol. Rapid Commun*., 2006, **27**, 430.

14 (a) H. Yuvaraj, M. H. Woo, E. J. Park, Y. T. Jeong and K. T. Lim, *Eur. Polym. J*., 2008, **44**, 637; (b) Q. Cheng, Y. He, V. Pavlinek, C. Li and P. Saha, *Synth. Met*., 2008, **158**, 953; (c) C. Xu, J. Sun and L. Gao, *J. Mater. Chem*., 2011, **21**, 11253.

15 (a) S. C. Wuang, K. G. Neoh, E. T. Kang, D. W. Pack and D. E. Leckband, *J. Mater. Chem*., 2007, **17**, 3354; (b) Z. Zhang, Q. Li, L. Yu, Z. Cui, L. Zhang and G. A. Bowmaker, *Macromolecules* 2011, **44**, 4610; (c) F. Deng and Y. X. Li, *Colloids Surf., A* 2012, **395**, 183.

16 (a) H. C. Kang and K. E. Gecheler, *Polymer* 2000, **41**, 6931; (b) J. Liu and M. X. Wan, *J. Mater. Chem*., 2001, **11**, 404; (c) S. Machida and S. Miyata. *Synthetic Metals*, 1989, **31**, 311; (d) J. Y. Ouyang and Y. F. Li, *Polymer* 1997, **38**, 1971

17 (a) G. M. Sheldrick, SHELX-97, Program for Crystal Structure Refinement; University of Göttingen, Germany, 1997; (b) G. M. Sheldrick, SHELX-97, Program for Crystal structure Solution; University of Göttingen, Germany, 1997.

18 (a) X. Wang, J. Peng, D. D. Wang, M. G. Liu, C. L. Meng, A. X. Tian, K. Alimaje and Z. Y. Shi, *Inorg. Chim. Acta*., 2012, **392**. 160; (b) Y. Lu, J. Lv, E. B. Wang, Y. Q. Guo, X. X. Xu and L. Xu, *J. Mol. Struct*., 2005, **740**, 159.

19 (a) X. F. Wang, Y. H. Shen, A. J. Xie, L. G. Qiu, S. Li and Y. Wang, *J. Mater. Chem*., 2011, **21**, 9641; (b) H. Zhang, R. L. Zong and Y. F. Zhu, *J. Phys. Chem. C* 2009, **113**, 4605.

20 (a) C. X. Zhang, Y. G. Chen, Q. Tang, Z. C. Zhang, D. D. Liu and H. X. Meng, *Inorg. Chem. Commun*., 2012, **17**, 155; (b) Y. Lu, Y.G. Li, E. B. Wang, J. Lv, L. Xu and R. Clérac, *Eur. J. Inorg. Chem*., 2005, 1239.

21 (a) S. X. Min, F. Wang and Y. Q. Han, *J. Mater Sci*., 2007, **42**, 9966; (b) J. H. Wei, Q. Zhang, Y. Liu, R. Xiong, C. X. Pang and J. Shi, *J. Nanopart. Res*., 2011, **15**, 3157; (c) S. De, A. Dey and S. K. De, *J. Phys. Chem. Solids* 2007, **68**, 66; (d) L. X. Zhang, P. Liu and Z. X. Su, *Polym. Degrad. Stab*., 2006, **91**, 2213.

22 (a) H. Liu, S. A. Cheng, M. Wu, H. J. Wu, J. Q. Zhang, W. Z. Li and C. N. Cao, *J. Phys. Chem. A* 2000, **104**, 7016; (b) W. H. Leng, Z. Zhang, J. Q. Zhang and C. N. Cao, *J. Phys. Chem. B* 2005, **109**, 15008.

23 (a) L. H. Ai, C. H. Zhang, L.L. Li and J. Jiang, *Appl. Catal. B* 2014, **148-149**, 191; (b) L. J. Shen, S. J. Liang, W. M. Wu, R. W. Liang and L. Wu, *Dalton Trans*., 2013, **42**, 13649; (c) X. H. Lu, G. M. Wang, S. L. Xie, J. Y. Shi, W. Li, Y. X. Tong, and Y. Li, *Chem. Commun*., 2012, **48**, 7717. (d) S. L. Xie, T. Zhai, W. Li, M. H. Yu, C. L. Liang, J. Y. Gan, X. H. Lu, and Y. X. Tong, *Green Chem*., 2013, **15**, 2434.

Table 1 Degradation efficiency of RhB with different photocatalysts

Photocatalyst	Condition	Time (hours)	η (%)
ZnP_2Mo_5NR	ultraviolet light irradiation	8	50.07
ZnP_2Mo_5NR	visible light irradiation	8	0.01
PPy(A)/ ZnP_2Mo_5NR	visible light irradiation	2	76.12
PPy(B)/ ZnP_2Mo_5NR	visible light irradiation	2	73.92
PPy(C)/ ZnP_2Mo_5NR	visible light irradiation	2	86.92
PPy(D)/ ZnP_2Mo_5NR	visible light irradiation	2	60.86
PPy(A)	visible light irradiation	6	59.07
PPy(B)	visible light irradiation	6	40.12
PPy(C)	visible light irradiation	6	35.82
PPy(D)	visible light irradiation	6	30.48
PPy(A)/ ZnP_2Mo_5NR(M)	visible light irradiation	6	50.85
PPy(B)/ ZnP_2Mo_5NR(M)	visible light irradiation	6	61.99
PPy(C)/ ZnP_2Mo_5NR(M)	visible light irradiation	6	64.72
PPy(D)/ ZnP_2Mo_5NR(M)	visible light irradiation	6	43.20

Figure Captions

Figure 1 (a) 1D chain structure of **ZnP_2Mo_5** (inset, the fundamental unit of **ZnP_2Mo_5**); (b) SEM picture of **ZnP_2Mo_5NR** (inset, EDX of **ZnP_2Mo_5NR**).

Figure 2 SEM picture of **PPy/ZnP_2Mo_5NR** (inset, EDX of **PPy/ZnP_2Mo_5NR**); (a) **PPy(A)/ZnP_2Mo_5NR**; (b) **PPy(B)/ZnP_2Mo_5NR**; (c) **PPy(C)/ZnP_2Mo_5NR**; (d) **PPy(D)/ZnP_2Mo_5NR**

Figure 3 (a) PXRD of **ZnP_2Mo_5** and **ZnP_2Mo_5NR**; (b) PXRD of **PPy/ZnP_2Mo_5NR**; (c) FTIR of **ZnP_2Mo_5NR** and **PPy/ZnP_2Mo_5NR**; (d) Enlarged FTIR of **ZnP_2Mo_5NR** and **PPy/ZnP_2Mo_5NR**.

Figure 4 (a) DRS of **ZnP_2Mo_5NR** and **PPy/ZnP_2Mo_5NR**; (b) Tauc plots **ZnP_2Mo_5NR** and **PPy/ZnP_2Mo_5NR**.

Figure 5 (a) Photocurrent spectra of **ZnP_2Mo_5NR** and **PPy/ZnP_2Mo_5NR** under ultraviolet light; (b) Photocurrent spectra of **ZnP_2Mo_5NR** and **PPy/ZnP_2Mo_5NR** under visible light. (c) Nynquist plots of **ZnP_2Mo_5NR** and **PPy/ZnP_2Mo_5NR** electrodes under visible light. (d) Enlarged Nynquist plots of **ZnP_2Mo_5NR** and **PPy/ZnP_2Mo_5NR** electrodes.

Figure 6 Degradation rate as the function of time: (a) by **ZnP_2Mo_5NR**; (b) by **PPy/ZnP_2Mo_5NR**; (c) by PPy; (d) by **PPy/ZnP_2Mo_5NR(M)**.

Figure 7 (a) Conductivities of PPy; (b) Cycling runs of the degradation of RhB in the presence of **PPy(C)/ZnP_2Mo_5NR**; (c) PXRD of recycled **PPy(C)/ZnP_2Mo_5NR**; (d) FTIR of recycled **PPy(C)/ZnP_2Mo_5NR**.

Figure 8 (a) Mott-Schotty plot of **ZnP_2Mo_5NR**; (b) Diagram of the photocatalytic mechanism for **PPy/ZnP_2Mo_5NR** under visible light.

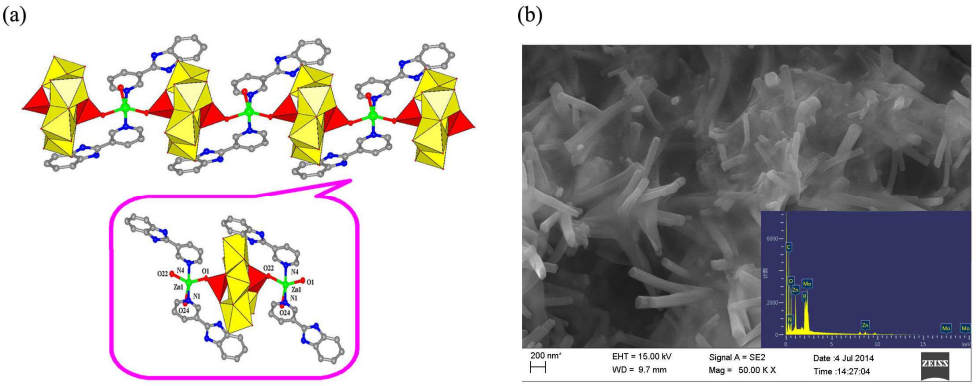
(a)
(b)
200 nm*
EHT = 15.00 kV
WD = 9.7 mm
Signal A = SE2
Mag = 50.00 K X
Date :4 Jul 2014
Time :14:27:04
ZEISS

Figure 1

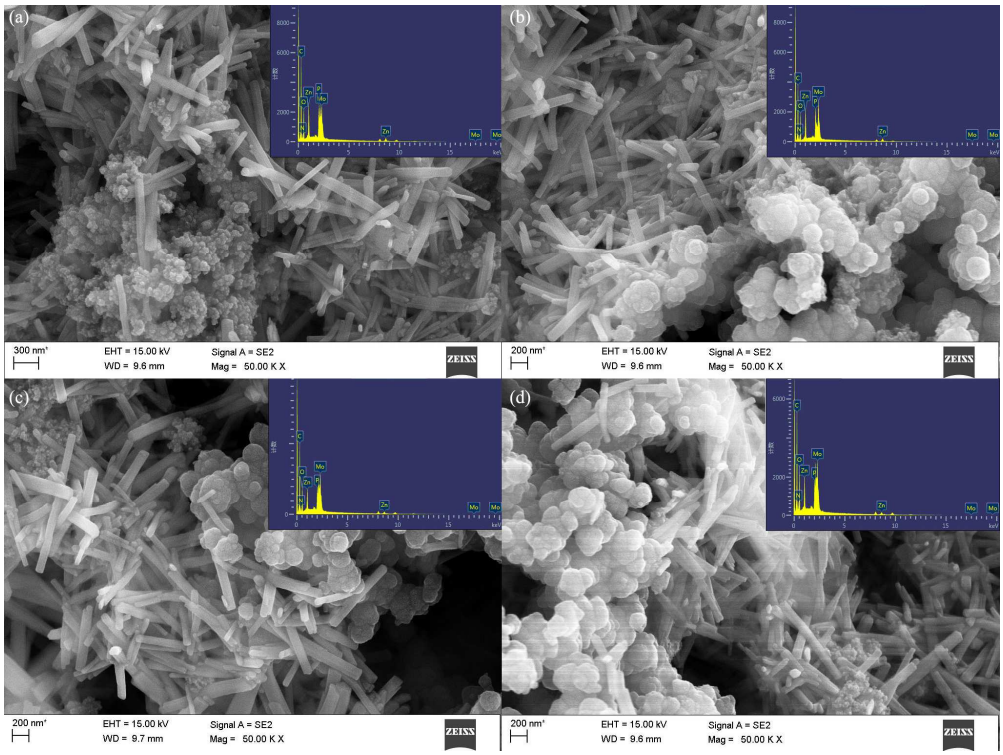
(a)
300 nm
EHT = 15.00 kV
WD = 9.6 mm
Signal A = SE2
Mag = 50.00 K X
ZEISS
(b)
200 nm
EHT = 15.00 kV
WD = 9.6 mm
Signal A = SE2
Mag = 50.00 K X
ZEISS
(c)
200 nm
EHT = 15.00 kV
WD = 9.7 mm
Signal A = SE2
Mag = 50.00 K X
ZEISS
(d)
200 nm
EHT = 15.00 kV
WD = 9.6 mm
Signal A = SE2
Mag = 50.00 K X
ZEISS

Figure 2

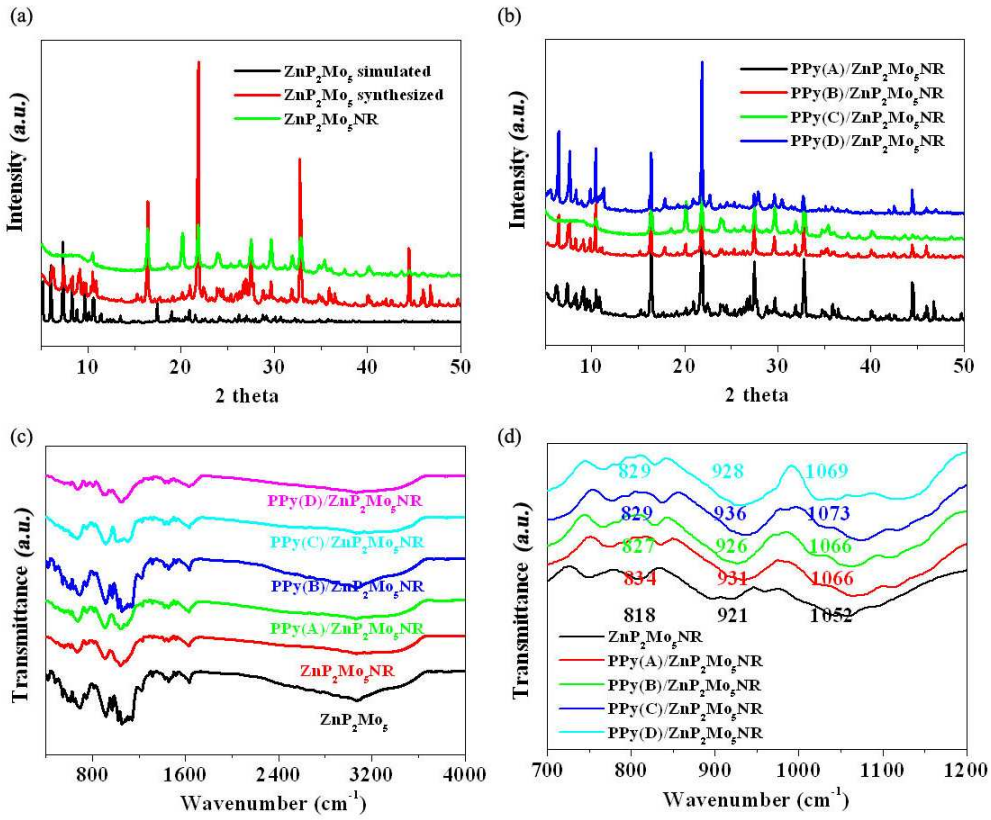
(a)
Intensity (a.u.)
2 theta
ZnP2Mo5 simulated
ZnP2Mo5 synthesized
ZnP2Mo5NR
(b)
Intensity (a.u.)
2 theta
PPy(A)/ZnP2Mo5NR
PPy(B)/ZnP2Mo5NR
PPy(C)/ZnP2Mo5NR
PPy(D)/ZnP2Mo5NR
(c)
Transmittance (a.u.)
Wavenumber (cm-1)
PPy(D)/ZnP2Mo5NR
PPy(C)/ZnP2Mo5NR
PPy(B)/ZnP2Mo5NR
PPy(A)/ZnP2Mo5NR
ZnP2Mo5NR
ZnP2Mo5
(d)
Transmittance (a.u.)
Wavenumber (cm-1)
829
928
1069
829
936
1073
827
926
1066
834
931
1066
818
921
1052
ZnP2Mo5NR
PPy(A)/ZnP2Mo5NR
PPy(B)/ZnP2Mo5NR
PPy(C)/ZnP2Mo5NR
PPy(D)/ZnP2Mo5NR

Figure 3

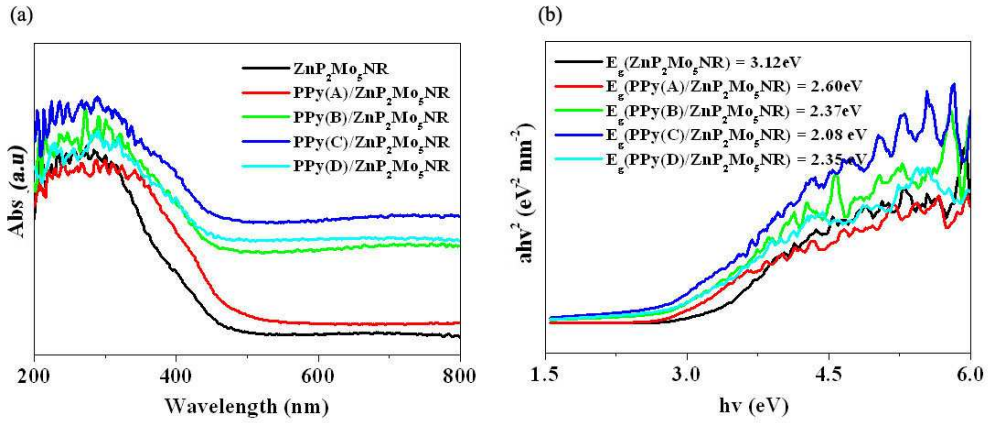
(a)
(b)
ZnP2Mo5NR
PPy(A)/ZnP2Mo5NR
PPy(B)/ZnP2Mo5NR
PPy(C)/ZnP2Mo5NR
PPy(D)/ZnP2Mo5NR
Abs (a.u)
Wavelength (nm)
200
400
600
800
Eg(ZnP2Mo5NR) = 3.12eV
Eg(PPy(A)/ZnP2Mo5NR) = 2.60eV
Eg(PPy(B)/ZnP2Mo5NR) = 2.37eV
Eg(PPy(C)/ZnP2Mo5NR) = 2.08 eV
Eg(PPy(D)/ZnP2Mo5NR) = 2.35 eV
ahv2 (eV-2 nm-2)
hv (eV)
1.5
3.0
4.5
6.0

Figure 4

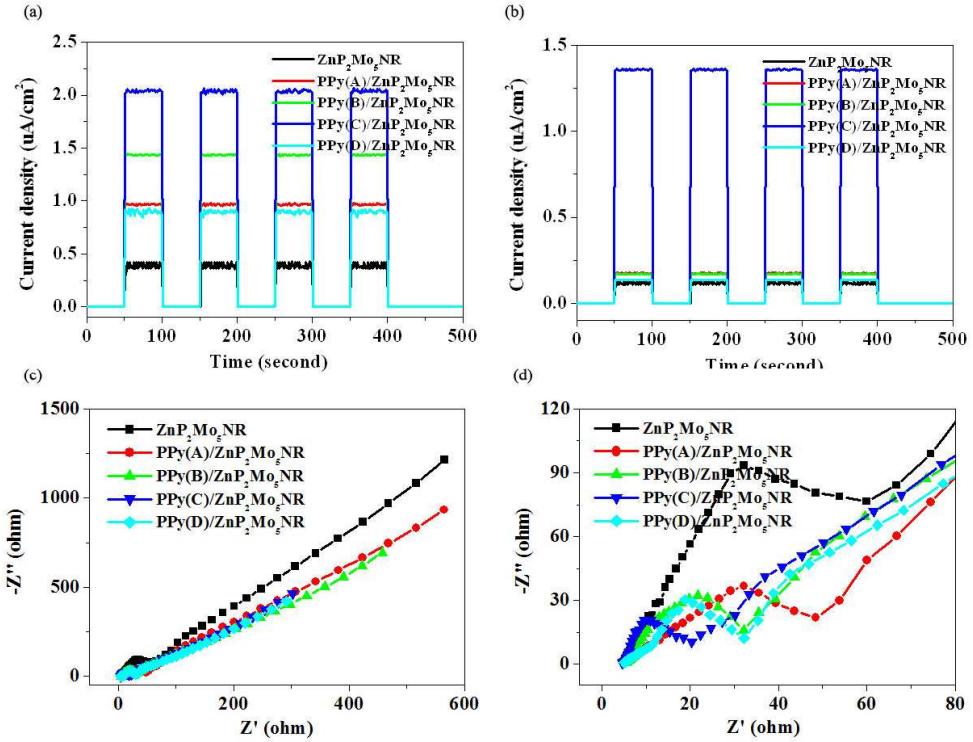
(a)
Current density (uA/cm^2)
Time (second)
ZnP$_2$Mo$_5$NR
PPy(A)/ZnP$_2$Mo$_5$NR
PPy(B)/ZnP$_2$Mo$_5$NR
PPy(C)/ZnP$_2$Mo$_5$NR
PPy(D)/ZnP$_2$Mo$_5$NR
(b)
Current density (uA/cm^2)
Time (second)
(c)
-Z'' (ohm)
Z' (ohm)
(d)
-Z'' (ohm)
Z' (ohm)

Figure 5

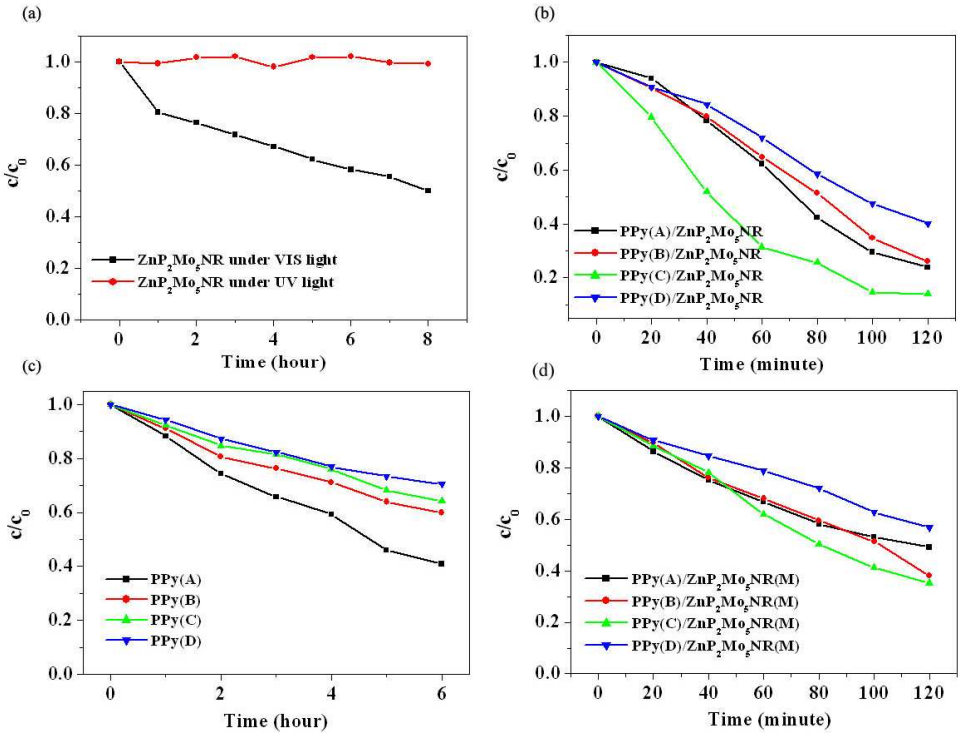
(a)
c/c0
Time (hour)
ZnP2Mo5NR under VIS light
ZnP2Mo5NR under UV light
(b)
c/c0
Time (minute)
PPy(A)/ZnP2Mo5NR
PPy(B)/ZnP2Mo5NR
PPy(C)/ZnP2Mo5NR
PPy(D)/ZnP2Mo5NR
(c)
c/c0
Time (hour)
PPy(A)
PPy(B)
PPy(C)
PPy(D)
(d)
c/c0
Time (minute)
PPy(A)/ZnP2Mo5NR(M)
PPy(B)/ZnP2Mo5NR(M)
PPy(C)/ZnP2Mo5NR(M)
PPy(D)/ZnP2Mo5NR(M)

Figure 6

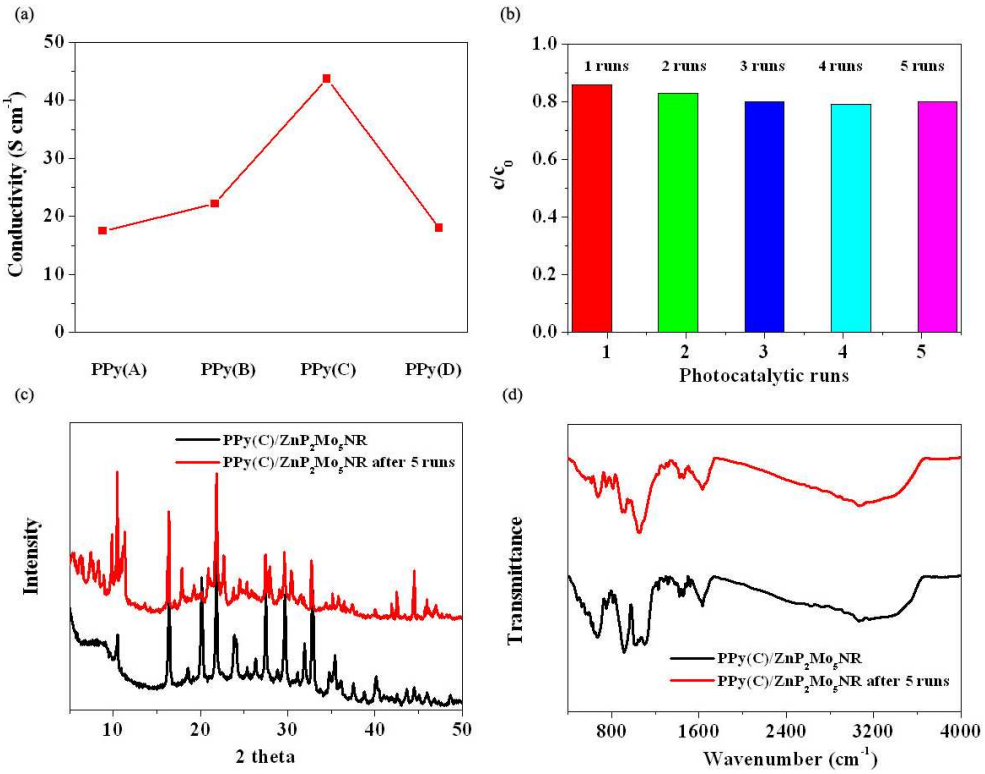
(a)
Conductivity (S cm-1)
PPy(A)
PPy(B)
PPy(C)
PPy(D)
(b)
c/c0
1 runs
2 runs
3 runs
4 runs
5 runs
Photocatalytic runs
(c)
Intensity
PPy(C)/ZnP2Mo5NR
PPy(C)/ZnP2Mo5NR after 5 runs
2 theta
(d)
Transmittance
PPy(C)/ZnP2Mo5NR
PPy(C)/ZnP2Mo5NR after 5 runs
Wavenumber (cm-1)

Figure 7

1

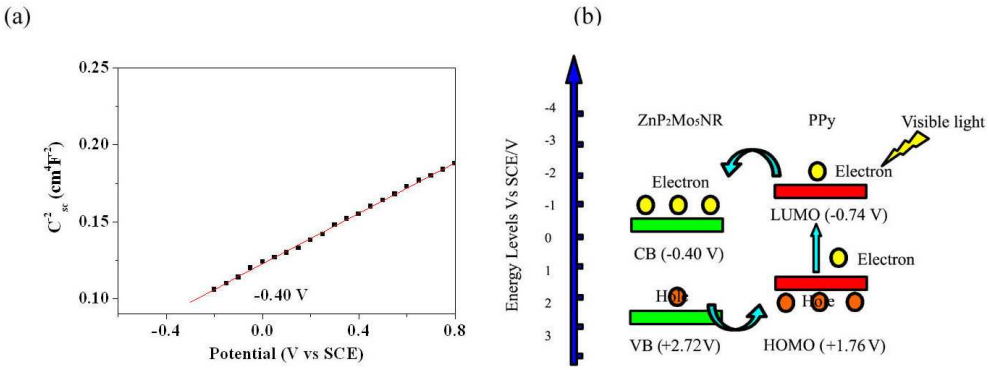
(a)
(b)
0.25
0.20
0.15
0.10
-0.40 V
-0.4
0.0
0.4
0.8
Potential (V vs SCE)
Energy Levels Vs SCE/V
-4
-3
-2
-1
0
1
2
3
ZnP2MoSNR
PPy
Visible light
Electron
Electron
LUMO (-0.74 V)
CB (-0.40 V)
Electron
VB (+2.72V)
HOMO (+1.76 V)

2

3 **Figure 8**